A two-electron reducing reaction of CO2 to an oxalate anion: a theoretical study of delocalized (presolvated) electrons in Al(CH3)n(NH3)m, n = 0–2 and m = 1–6, clusters

esmail alikhani, Benjamin Janesko

Two electron reducing reaction of CO_2 to oxalate anion: theoretical study of delocalized (presolvated) electrons in $Al(CH_3)_n(NH_3)_m$, n = 0 – 2 and m = 1 – 6, clusters

Mohammad Esmail Alikhani [a] and Benjamin G. Janesko [b]

a. Sorbonne Universités, MONARIS, CNRS-UMR 8233, 4 place Jussieu, 75005 Paris Cedex 05, France.
E-mail : esmail.alikhani@sorbonne-universite.fr ID: https://orcid.org/0000-0001-8412-4147

b. Department of Chemistry & Biochemistry, Texas Christian University, 2800 S. University Dr, Fort Worth, TX, USA
E-mail: b.janesko@tcu.edu ID: https://orcid.org/0000-0002-2572-5273

Abstract

Presolvated electron possibility in three oxidation states of aluminum –Al(0), Al(I), and Al(II)– has been theoretically investigated for the $Al+6NH_3$, $Al(CH_3)+5NH_3$, and $Al(CH_3)_2+4NH_3$ reactions. It has been shown that the metal center adopts a tetrahedral shape for its most stable geometric structure, whatever the degree of Al oxidation state. Using different analysis techniques (highest occupied molecular orbital shapes, spin density distribution, and electron delocalization range), we showed that we have shown that presolvated (delocalized) electrons are only formed in the $Al(CH_3)_2(NH_3)_p$ coordination complexes when $2 \leq p \leq 4$. It has also been evidenced that these delocalized electrons being powerful reducing agent allowed two CO_2 molecules to be captured and forming an oxalate ion in close contact with $[Al_2(CH_3)_2(CH_2)_2(NH_3)_4]^{2+}$ dication core.

Keywords

Solvated electron precursor, electron delocalization range, ELF topology, tetrahedral aluminum center, carbon dioxide reduction, Oxalate ion

TOC:

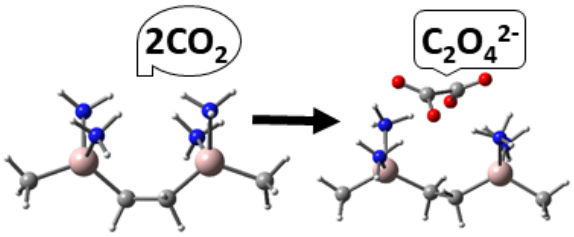

Two e⁻ reducing of CO_2 to oxalate anion

I. Introduction

It has been well known, since the early years of the nineteenth century, that the alkali metal solvation in ammonia significantly displaces the alkali valence electron from the metal center, which leads to confined electrons by the solvent shell.[1–3]

Over the last few decades, numerous experimental [4–7] and theoretical [8–16] studies have addressed not only the solubility of different metals [4,15,17–24] in NH_3 but also the role of different solvents in the formation of solvated electrons. [25–28] The study of solvated metals in NH_3 has recently been applied to some transition metals.[21–23] Experimental and theoretical works have evidenced that the solvation of metals in different solvents (ammonia, water, and tetrahydrofuran (THF), for example) give rise to the three categories of solvated species: tetracoordinated complexes such as $Li(NH_3)_4$,[6,18,29] hexacoordinated species such as $Na(NH_3)_6$,[17,30] and octacoordinated compounds such as $Y(NH_3)_8$.[22]

Several works have been devoted to understanding and rationalizing the process of solvated electron formation during alkali metal solvation in ammonia.[8,10,20,30,31] In the case of $Na(THF)_6$,[30,31] the valence electron 3s loses its spherical symmetry as the number of THFs encircling the neutral Na atom increases from 1 to 6. The main cause of this deformation is indeed the Pauli repulsion between the valence electron of Na and the O lone pair electrons. Thanks to this repulsion, the valence electron of Na is pushed back in the opposite direction to the Na–O dative bond formation. The valence electron exhibits a three-dimensional fan shape (skullcap) located on the opposite side of four tetrahydrofuran molecules in $Na(THF)_4$, which again gets its spherical shape in $Na(THF)_6$.[31] Miliordos and co-workers, in a systematic investigation on the nature of supermolecular bonds, showed that such a molecular complex mimics a super-atom whose valence electron is distracted in a super-orbital (outer orbital).[13,20,23,32] For instance, the neutral $Mg(H_2O)_6$ complex in its ground electronic state should be considered as a dication $Mg(H_2O)_6^{2+}$ core in tight contact with two electrons accommodated near the coordinated water molecules.[18] In this sense, a solvated electron distributed in the periphery of ligands in dative interaction with the cationic core differs from the proton encircled within a molecular building bloc.[33,34] Such molecular clusters were called

"solvated electron precursors" (SEPs) for the first time by Miliordos and co-workers.[15]

To the best of our knowledge, dissolving aluminum in ammonia by electrolysis has only been mentioned once in a communication to the editor.[35,36] We found no other experimental or theoretical work in the literature about the solvation of Al in NH_3 forming solvated cations and solvated electrons.

The purpose of the present work is to extend the study of the solvated electrons to the molecular compounds containing Al, $Al(CH_3)$, and $Al(CH_3)_2$ in interaction with ammonia. Our study will focus on three questions: 1) for each of the three systems, what is the maximum number of NH_3 in the first coordination shell? In other words, can we have hexacoordinated aluminum? 2) For the most stable structure of each system, do the valence electrons of Al remain localized on the metallic center, or delocalized to the periphery of NH_3? 3) Can we use these delocalized electrons as reducing agent to capture and activate CO_2 molecule?

II. Computational details

All first principles calculations were performed using the Gaussian 09 or Gaussian 16 quantum chemical packages.[37,38] Optimization of the stationary points on the potential energy surface was performed using density functional theory with Handy's long-range corrected version of B3LYP exchange-correlation functional [39–43] including the D3 version of Grimme's dispersion with Becke-Johnson damping (GD3BJ) [44], noted as CAM-B3LYP-GD3BJ in this paper. The Pople triple-ζ quality basis set extended with polarization and diffuse functions, 6-311++G (2d, 2p) has been used for all atoms.[45,46] Selected calculations use Hartree-Fock theory (HF), second-order many-body perturbation theory (MP2), or complete active space self-consistent field (CASSCF) methods at CAM-B3LYP geometries.

To analyze the structure of solvated electrons in real space, we used two topological approaches: the EDR (electron delocalization range) [47–49] and the ELF (electron localization function).[50] The EDR and ELF are two complementary techniques that allow us to quantify the diffuse character of solvated electron (EDR), and measure the degree of electronic localization (ELF) within a chemical compound. The ELF is large (near 1) in regions that have single-electron character, and small (near zero) in regions such as core-valence overlap regions.

The EDR(***r;d***) is the expectation value of a nonlocal one-electron operator, namely, the projection of the system's wavefunction onto a normalized one-electron Gaussian function centered at point ***r*** with Gaussian exponent d^{-2}. In regions where this overlap is near 1, the electronic structure about point ***r*** is dominated by orbitals delocalized over distance *d*. We quantify this using the orbital overlap distance D(***r***), defined as the distance *d* maximizing EDR(***r;d***). Plots of electron density isosurfaces, colored with the value of D(***r***), highlight regions of space containing delocalized electrons. For the ELF topological analysis, the partition of the molecular space in terms of nonoverlapping space-filling domains has been performed using the TopMod package. [51] The EDR and overlap distance are evaluated using the Multiwfn package [52] or the Gaussian 16 package.[38]

III. Results and discussion

Recently, by pure analogy with the results obtained for the $Be(NH_3)_4$ complex, Miliordos and co-workers suggested that $Al(NH_3)_x$ should be hexacoordinated which could host three outer electrons.[15] Therefore, we focus our investigation on three types of systems in which aluminum is surrounded by six molecules, but with different degrees of oxidation: $Al(NH_3)_6$, $Al(CH_3)(NH_3)_5$, and $Al(CH_3)_2(NH_3)_4$. Before starting the discussion, let us note here the color code used in this paper to distinguish different atoms illustrated in different figures, as follows: the pink spheres represent an aluminum atom, blue spheres a nitrogen atom, white spheres a hydrogen atom, red spheres an oxygen atom, and gray spheres a carbon atom.

A. Al(0) in interaction with six NH_3 molecules

All the optimized structures and corresponding relative energies of the neutral $Al(NH_3)_6$ are shown in Figure 1.

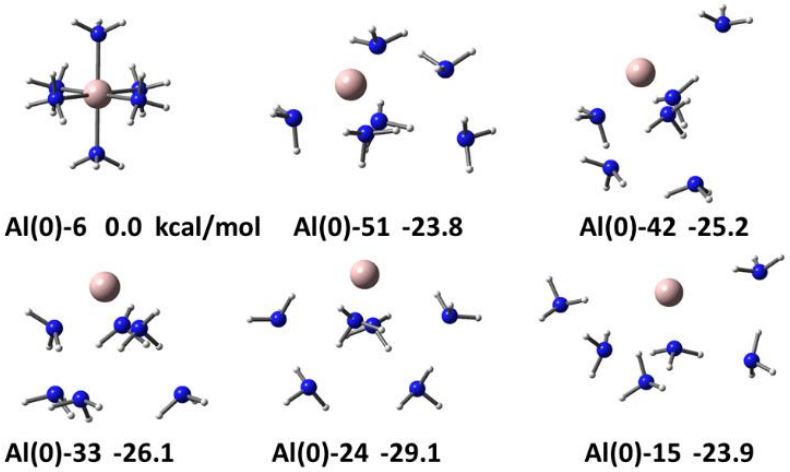

Figure 1. Optimized structures and relative energies (in kcal/mol) of the $Al(NH_3)_6$ compound.

Starting from six initial geometries, we found 4 classes of structures:

- Hexacoordinated Al (noted as Al(0)-6)
- Three tri-coordinate structures were obtained by optimizing three structures initially penta-, tetra-, and tricoordinates, respectively noted as Al(0)-51, Al(0)-42, and Al(0)-33 in Figure 1.
- Two structures Al(0)-24 and Al(0)-15 show respectively the two optimized di- and mono-coordinated Al.

As shown by the relative energy reported in Figure 1, the dicoordinated complex Al(0)-24 corresponds to the global minimum on the potential energy hyper-surface. The mono- and tri-coordinated local minima (Al(0)-15, Al(0)-33, Al(0)-42, and Al(0)-51) are placed a few kcal/mol (3 – 5 kcal/mol) above the global minimum. The hexacoordinated species is much less stable than the other 5 structures. In the Al(0)-24 structure, only two NH_3 molecules, in dative bonding with the Al atom, form the first solvation sphere, while the other fourth NH_3 molecules, forming hydrogen bonds with the other NH_3, constitute the second solvation shell.

In contrast to the case of hexacoordinated sodium atom by tetrahydrofuran – $Na(THF)_6$ – for which the average interaction energy per ligand (AIE) between Na and O (E_{int}/n) remains unchanged when the number of ligand increases from one to six,[30] the AIE is almost divided by three in going from $Al(NH_3)$ – $E_{int}/1$ = 11.2 kcal/mol – to $Al(NH_3)_6$ – $E_{int}/6$ = 4.5 kcal/mol. Our energetic results are in agreement with conclusions obtained in an electron paramagnetic

resonance study of the $Al(NH_3)$ compound. It was concluded that the codeposition of Al atoms with neat NH_3 gave only an olive-green deposit assigned to the di-coordinated species.[53] Our conclusion is also in agreement with the fact that only two adduct species $Al(NH_3)$ and $Al(NH_3)_2$ have been observed during the thermal reaction between Al and NH_3 using matrix infrared spectroscopy.[54]

To analyze the fate of the three valence electrons of Al within the Al(0)-24 complex, the contours of the two highest occupied molecular orbitals (HOMO and SOMO), as well as the ELF topological domains, are depicted in Figure 2.

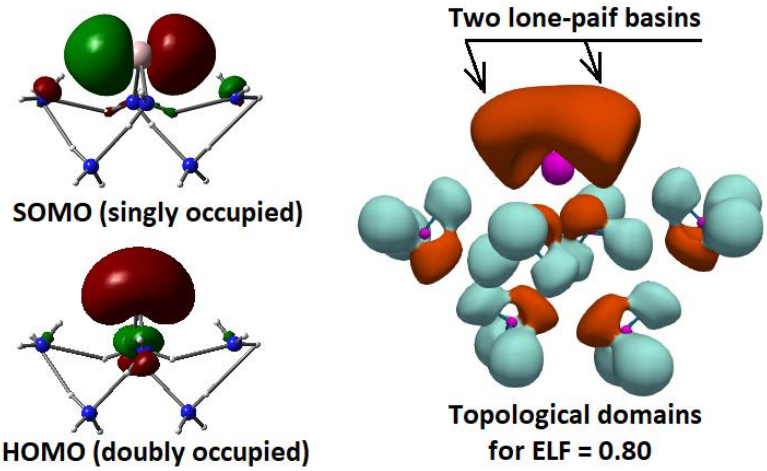

Figure 2. Contours of the two highest occupied molecular orbital (left panel) and the ELF domains (right panel) of the Al(0)-24 structure.

Both HOMO (doubly occupied) and SOMO (simply occupied) are highly localized on the metal atom. While HOMO has retained its atomic valence shape (3p), the 3s atomic orbital has been transformed upon formation of the complex into a highly polarized orbital oriented away from NH_3s. Consequently, we can stand that there is no diffuse (presolvated) electron in this compound. Additionally, the ELF topological domains show that two lone-pair basins with two Al-N dative bonding constitute a tetrahedral structure around the metal center. Assuming this quasi-VSEPR (valence shell electron pair repulsion), one would expect to obtain a tetrahedral structure upon optimization of $Al(NH_3)_6^+$ cation formed by lone pair electrons and three dative Al–N bonds. Our optimization calculations show that the global minimum on the potential energy surface of $Al(NH_3)_6^+$ is actually a tetrahedral structure as predicted by the model (see

Cartesian coordinates in SI). The calculated ionization potential (3.1 eV) is very close to its experimental value (3.09 ±0.06 eV).[55]

The electron delocalization range function EDR(***r;d***) is the expectation value of a nonlocal one-electron operator, namely, the overlap between the system's wavefunction and a one-electron Gaussian function centered at point **r** with Gaussian exponent d. In regions where this overlap is large (i.e., near 1), the electronic structure about point **r** is dominated by orbitals delocalized over distance d. The overlap distance D(***r***) is defined as the distance d maximizing the EDR at point ***r***. In regions of a molecule where D(***r***) is large, the electronic structure is dominated by delocalized electron density.

Figure 3 shows the orbital overlap distance D(***r***) computed for Al(0)-24. The figure depicts the 0.001 electrons/bohr^3 density isosurface of the neutral Al(0)-24 complex, with each point **r** on the surface colored by the value of the overlap distance D(***r***), ranging from 2.5 au (red) to 5 au (blue). The overlap distance is around 2.5 bohr on the ammonia molecules, increasing to >5 bohr in the region corresponding to the weakly bound electrons. For comparison, the right panel of Figure 3 shows the overlap distance computed for isolated NH_3 and an isolated neutral non-spherical doublet aluminum atom. From this perspective, the valence electrons of the Al(0)-24 complex are localized in diffuse orbitals on the aluminum. The electron density in the region of the frontier orbitals largely arises from diffuse and weakly bound electrons.

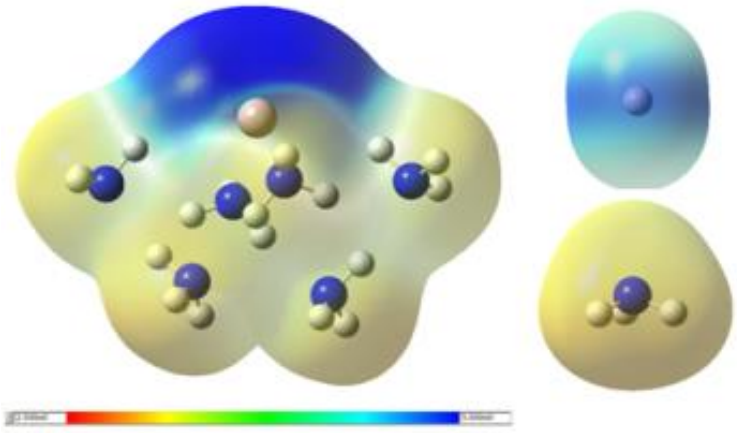

Figure 3. Orbital overlap distance of the Al(0)-24 structure (left) compared to isolated neutral singlet nonspherical Al atom (right top) and isolated NH_3 (right bottom). Blue regions denote delocalized electron density.

The above discussion revealed that ammonia ligand cannot displace any of the three Al valence electrons in the ground state of $Al(NH_3)_6$ molecular clusters. In order to modify the number of valence electrons available on Al, we will study the dissolution of $Al(CH_3)$ and $Al(CH_3)_2$ in NH_3. Following the formation of Al-C polar bond, the metal center oxidizes to Al(I) and Al(II) within the two compounds $Al(CH_3)$ and $Al(CH_3)_2$, respectively. Furthermore, the addition of methyl radical also allows us to connect several metal centers by building hydrocarbon chain with several carbon atoms.

B. Al(I) in interaction with five NH_3 molecules

$Al(CH_3)$ has a polarized lone pair electrons located on the metal atom. The two most interesting isomers arising from the $Al(CH_3)+5NH_3$ reaction are illustrated in Figure 4. The global minimum of $Al(CH_3)(NH_3)_5$ Is a dicoordinated structure that is located by 13 kcal/mol below the pentacoordinated isomer.

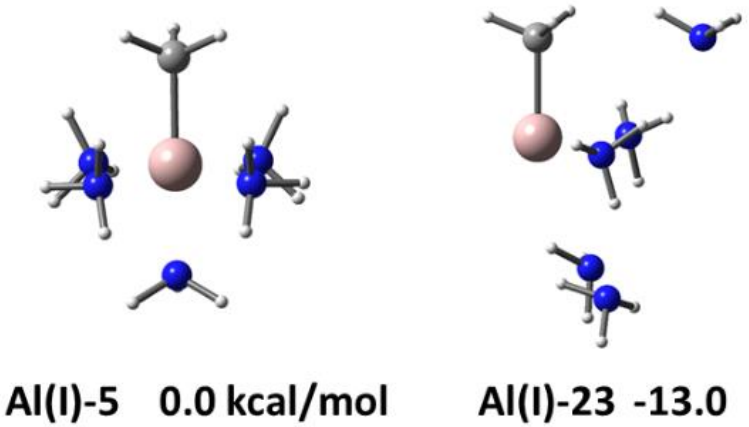

Figure 4. Optimized structures and relative energies (in kcal/mol) of two relevant isomers of $Al(CH_3)(NH_3)_5$.

For the global minimum Al(I)-23, Figure 5 reveals two interesting properties:

- The highest molecular orbital (left panel) a pair of electrons is essentially centered on the aluminum atom,
- As illustrated by the ELF localization domains (right panel), one C–Al polar covalent bond, two Al–N dative bonds, and one lone pair electrons of Al constitute a tetrahedral structure around Al atom.

Consequently, we can conclude that there is no delocalized (presolvated) electrons in the global minimum of $Al(CH_3)(NH_3)_5$ coordination complex.

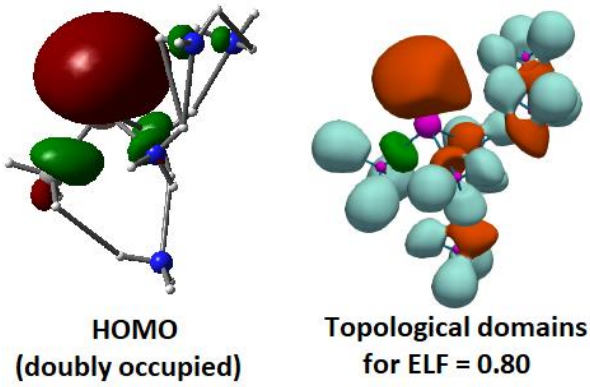

Figure 5. Contours of the highest occupied molecular orbital (left panel) and the ELF domains (right panel) of the Al(I)-23 structure.

C. Al(II) in interaction with four NH_3 molecules

In the previous two sections, we showed that the dative interactions Al–N are not strong enough to overcome the attachment energy of the non-bonding electrons of the metal center not to ionize the complex but to push them to the peripheral of the ligands so that the (Al^+, e^-) tight-contact pair energetically becomes the global minimum. What about the $Al(CH_3)_2$+$4NH_3$ reaction? Will the single non-bonding electron highly located on Al in the $Al(CH_3)_2$ reactant give way to an NH_3 molecule within the global minimum of $Al(CH_3)_2(NH_3)_4$?

The three most interesting isomers arising from the $Al(CH_3)_2$+$4NH_3$ reaction are illustrated in Figure 6.

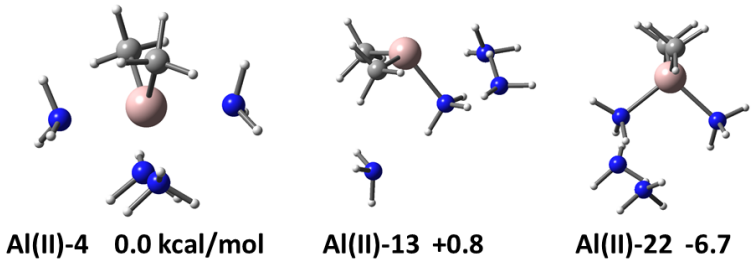

Figure 6. Optimized structures and relative energies (in kcal/mol) of the relevant isomers of $Al(CH_3)_2(NH_3)_4$.

Within the global minimum structure, Al(II)-22, the Al(II) metal center is effectively in a dative bond with two NH_3 molecules, while the other two NH_3 constituting the second solvation sphere form hydrogen bonds with the first two NH_3. Correspondingly, the two Al–N dative bonds together with two Al–C polar covalent bonds form a tetrahedral structure around the metal center.

Is the single non-bonding electron always located on the metal center? As illustrated by the contour of the singly occupied molecular orbital (see Figure 7 left panel), it is no longer localized on Al but is distributed on peripheral NH_3s. The ELF topology (see Figure 7 right panel) also found a peripheral basin placed near the hydrogen atoms of the two NH_3s of the second solvation shell. However, it should be emphasized that because of the diffuse (delocalized) nature of this electron, the ELF topology is not able to well describe the topological domain attributed to this solvated electron. Indeed, we find by the ELF topology a basin dedicated to this delocalized electron, but the synaptic order as well as the population of this basin remains very poorly defined. In contrast, the EDR analysis is perfectly suited to quantify the diffuse character of such an electron.

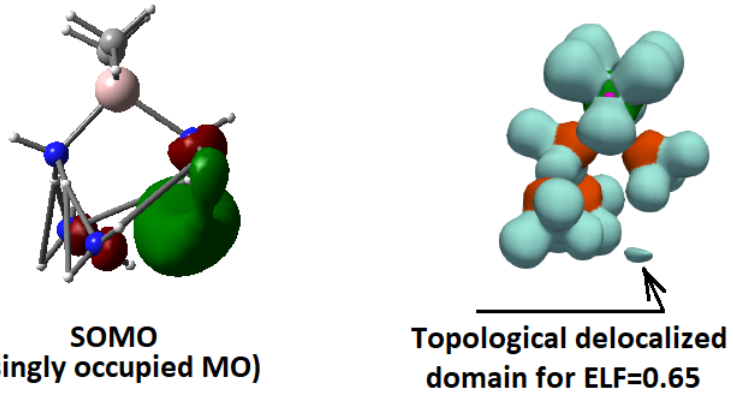

Figure 7. Contours of the singly occupied molecular orbital (left) and the ELF domains (right) with ELF=0.65 of the Al(II)-22 structure.

Figure 8 shows the orbital overlap distance D(***r***) of the Al(II)-22 structure. The left panel depicts the 0.001 electrons/bohr^3 density isosurface, with each point ***r*** on the surface colored by the value of the overlap distance D(***r***), ranging from 2.5 au (red) to 7 au (blue). The right panel displays the isosurfaces EDR(***r***;*d*)=0.7, computed for d=2.5 au (blue surface) and d=6 au (red

surface). Both measures confirm the substantially delocalized electron density separate from the metal atom.

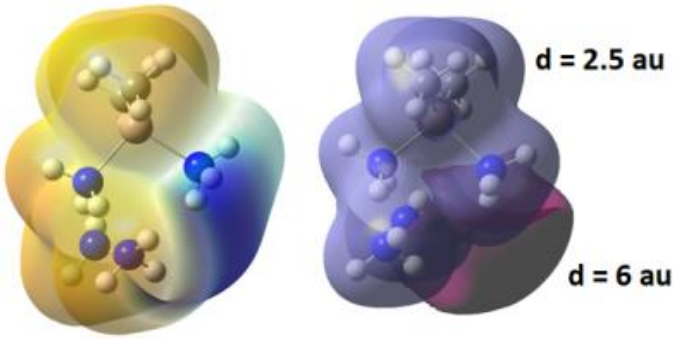

Figure 8. Orbital caption: Orbital overlap distance (left) and electron delocalization range at two representative distances d(right) of the Al(II)-22 structure.

Therefore, the global minimum of $Al(CH_3)_2(NH_3)_4$ should be described as a (cationic $Al(CH_3)_2(NH_3)_4^+$ core / delocalized e^-) pair, belonging to the SEPs family.[15,21]

D. Some ideas for extension and application

Inspired by a recent work on $(CH_3)B(NH_3)_3$ and its extension following the aliphatic chain $(NH_3)_3B(CH_2)_{3-6}B(NH_3)_3$,[19] we consider here $Al_2(CH_3)_2(CH_2)_2(NH_3)_4$ resulting from the linkage of two $Al(CH_3)_2(NH_3)_2$ monomers via an aliphatic hydrocarbon bridge.

For this system containing two metal centers, the singlet state is calculated to be more stable than the triplet one by 8.1 kcal/mol (see SI). As illustrated in Figure 9, two valence electrons of aluminum coupled into a singlet state are delocalized and distributed on the outer parts of NH_3s, forming a SEP compound.[19]

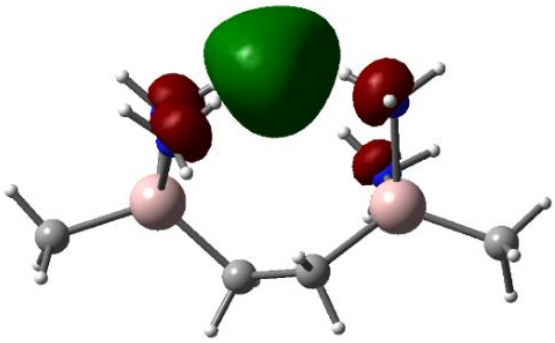

HOMO (doubly occupied)

Figure 9. Contour of the highest occupied molecular orbital of the global minimum (singlet spin state) of $Al_2(CH_3)_2(CH_2)_2(NH_3)_4$.

Figure 10 shows the orbital overlap distance computed for the singlet and triplet states of the two-metal-center $Al_2(CH_3)_2(CH_2)_2(NH_3)_4$ system. The figure depicts the 0.001 electrons/bohr^3 density isosurface, with each point ***r*** colored by the value of the overlap distance D(***r***), ranging from 2.5 au (red) to 8 au (blue). Singlet and triplet states both show a delocalized electron density region on the amine groups' outer parts. However, the singlet-coupled species displays substantially larger delocalization lengths, corresponding to a deep blue color, and consistent with a delocalized bonding-type orbital.

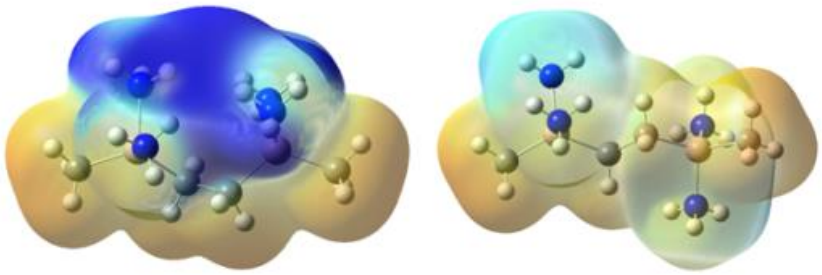

Figure 10. Orbital overlap distance computed for the singlet and triplet states of the two-metal-center $Al_2(CH_3)_2(CH_2)_2(NH_3)_4$ system.

Figure 11 shows the orbital overlap distance computed for Al(0)-24 at three different levels of theory: CAM-B3LYP DFT (left), Hartree-Fock theory (center), and second-order many-body perturbation theory (MP2) (right). The figure depicts the 0.001 electrons/bohr^3 density isosurface of the neutral Al(0)-24 complex, with each point ***r*** on the surface colored by the value of the overlap distance D(***r***), ranging from 3 au (red) to 5 au (blue). Calculations use the DFT geometry from above. Each figure is labeled with the computed vertical electron binding energy. CAM-B3LYP DFT predicts the strongest electron binding, but also predicts that the solvated electron is relatively delocalized, visible as a darker blue color in the solvated electron region. Hartree-Fock and MP2 calculations predict more compact structures for the solvated electron. This is consistent with significant density-driven error in DFT calculations on solvated electrons.[56]

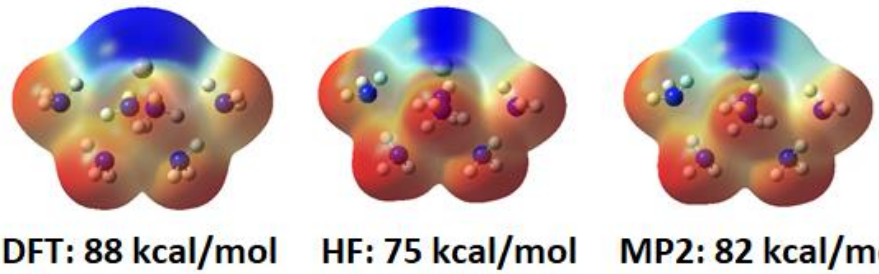

Figure 11. Orbital overlap distance computed for Al(0)-24 at three different levels of theory: CAM-B3LYP DFT (left), Hartree-Fock theory (center), and second-order many-body perturbation theory (MP2) (right).

Figure 12 show the orbital overlap distance for singlet $Al_2(CH_3)_2(CH_2)_2(NH_3)_4$ at four different levels of theory: CAM-B3LYP DFT, Hartree-Fock theory, second-order many-body perturbation theory (MP2), and multireference (two-electron two-orbital) CASSCF. The figure depicts the 0.001 electrons/bohr^3 density isosurface of the neutral complex, with each point ***r*** on the surface colored by the value of the overlap distance D(***r***), ranging from 3 au (red) to 8.5 au (blue). Each figure is labeled with the computed average vertical electron binding energy of the two solvated electrons. The bound electron pair is significantly more delocalized than the single solvated electron in Figure 11, with a large overlap distance around 8 bohr. In another contrast to Figure 11, the bound electron pair experiences a degree of "strong" electron correlation. (Spin symmetry breaking stabilizes the HF wavefunction by 7 kcal/mol). Both DFT and Hartree-Fock theory predict that the solvated electron pair is relatively delocalized, visible as a dark blue color in the solvated electron region. MP2 and CASSCF calculations both predict more compact structures for the solvated electron pair. However, both CASSCF and MP2 predict relatively weak binding energies compared to the DFT calculations. This differs from the density-driven error visible in Figure 11, and motivates further studies using correlated multireference wavefunction approaches.

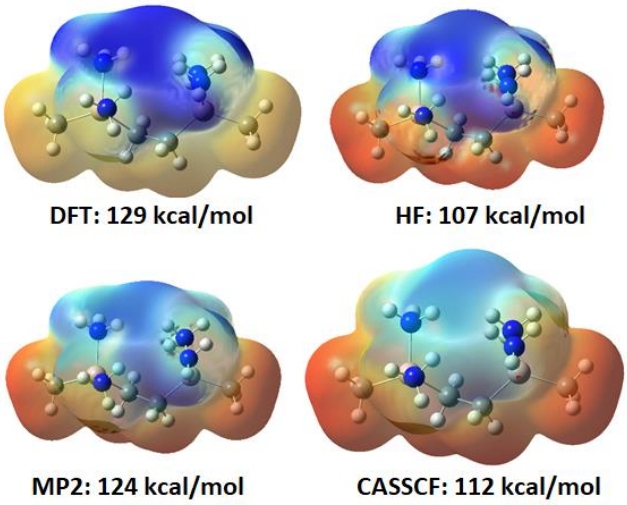

Figure 12. Orbital overlap distance computed for singlet $Al_2(CH_3)_2(CH_2)_2(NH_3)_4$ at four different levels of theory.

Let us devote the last paragraph of this work to the interaction of the CO_2 molecule with $Al_2(CH_3)_2(CH_2)_2(NH_3)_4$ compound. It is needless to underling that reducing CO_2 emissions into the atmosphere by CO_2 capture and conversion into value-added products is currently a highly attractive hot topic for all scientists. A very high number of publications in 2023 testifies to the high level of activity of researchers in this field. [57–62]

The approach of two CO_2 molecules to the $Al_2(CH_3)_2(CH_2)_2(NH_3)_4$ compound could lead to a two-electron reduction reaction of CO_2 in the singlet state and thus the formation of the C-C bond. The chemical compound containing two activated CO_2 at the triplet state is calculated to be less stable than the product in the singlet state by 56.8 kcal/mol (see Figure 13, and SI for structural information).

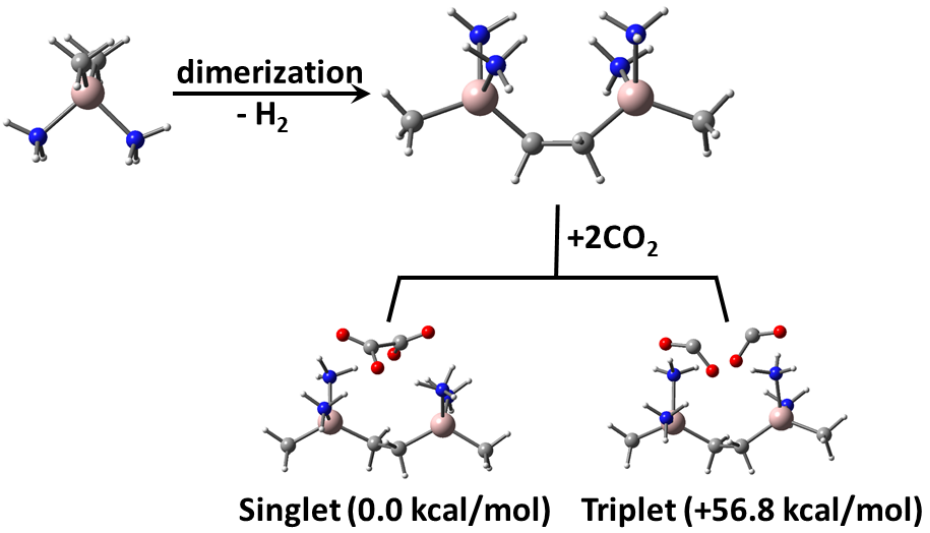

Figure 13. Schematic one electron and two electrons reduction reaction of two CO_2.

As shown in Figure 13, two CO_2 molecules are activated in the triplet state without forming an oxalate ion, and system is actually composed of three subunits: two bent $CO_2^{\bullet-}$ ion-molecules and one $[Al_2(CH_3)_2(CH_2)_2(NH_3)_4]^{2+}$ dication. Energetic stability between the three subunits is essentially ensured by hydrogen bonds formed between each $CO_2^{\bullet-}$ ion-molecule and the hydrogen atoms of amine groups of the dicationic core.

In the case of singlet state, the ELF topological analysis clearly shows that the population of the V(C, C) disynaptic basin rises to 2.3 e, characteristic of a single C-C bond (see Figure 14).

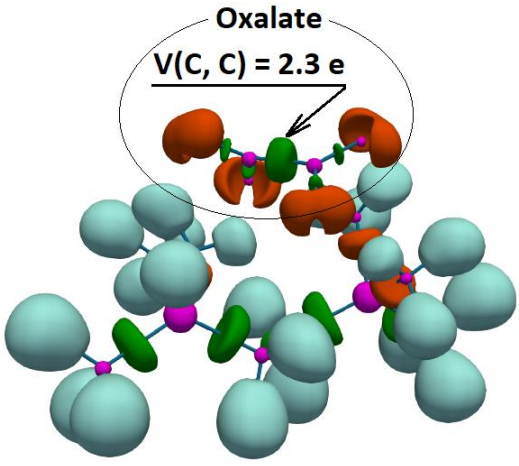

Figure 14. The ELF topological domains (ELF=0.85) of the $Al_2(CH_3)_2(CH_2)_2(NH_3)_4(CO_2)_2$ product at the singlet spin state.

In addition, the net charge of the new species $O_2C–CO_2$ calculated within the ELF formalism being equal to -1.8 e, indicates the formation of an oxalate ion, $C_2O_4^{2-}$. Therefore, we should

consider the final product in the singlet state as a pair of ions: oxalate ion in close contact with $[Al_2(CH_3)_2(CH_2)_2(NH_3)_4]^{2+}$ dication core. The oxalate ion desorption is highly endothermic by 384 kcal/mol.

IV. Conclusions

In the present work, we investigated the structural and energetic properties of three classes of coordination complexes: $Al(NH_3)_6$, $Al(CH_3)(NH_3)_5$, and $Al(CH_3)_2(NH_3)_4$. The global minimum of each class of systems has a tetrahedral structure around the metal center. In other words, the aluminum atom does not admit a hexacoordinated structure as long as the metal center can contribute one, two, or three electrons to the coordination complexes. We have thus only two NH_3s in the first solvation shell, while the other NH_3s make up the second shell. Based on the SOMO/HOMO orbital properties and EDR analysis, we were able to identify the presence of a diffuse electron only in the case of the global minimum of $Al(CH_3)_2(NH_3)_4$ far from aluminum center and almost localized into the peripheral of the second solvation shell, being thus a solvated electron precursor (SEP). However, the valence electrons of Al constitute the lone-pair electrons of the two other coordination complexes, $Al(NH_3)_6$, and $Al(CH_3)(NH_3)_5$, which are highly localized on the Al center.

Theoretical study of the extended $Al_2(CH_3)_2(CH_2)_2(NH_3)_4$ compound showed that the two delocalized electrons originating from the valence electron of Al centers couple in a singlet ground state. Delocalized lone-pair electrons could facilitate a two-electron reduction reaction when two CO_2 molecules interact with the extended compound in the singlet potential energy surface. Based on the ELF topological properties, we could identify the formation of an oxalate $C_2O_4^{2-}$ ion.

Author Contributions

Mohammad Esmaïl Alikhani: Optimization calculations, ELF analysis, and writing the original draft

Benjamin G. Janesko: Electronic and EDR analysis, and writing the original draft

Conflicts of interest

There are no conflicts to declare.

Electronic Supplementary Information (ESI)

An ESI file available

Notes and references

1 S. J. M. Thomas, P. P. Edwards and V. L. Kuznetsov, Sir Humphry Davy: Boundless Chemist, Physicist, Poet and Man of Action, *ChemPhysChem*, 2008, **9**, 59–66.

2 E. Zurek, P. P. Edwards and R. Hoffmann, A Molecular Perspective on Lithium-Ammonia Solutions, *Angewandte Chemie International Edition*, 2009, **48**, 8198–8232.

3 D.-F. Feng and L. Kevan, Theoretical models for solvated electrons, *Chem. Rev.*, 1980, **80**, 1–20.

4 R. Catterall and N. F. Mott, Metal-ammonia solutions, *Advances in Physics*, 1969, **18**, 665–680.

5 D. T. Elg, H. E. Delgado, D. C. Martin, R. M. Sankaran, P. Rumbach, D. M. Bartels and D. B. Go, Recent advances in understanding the role of solvated electrons at the plasma-liquid interface of solution-based gas discharges, *Spectrochimica Acta Part B: Atomic Spectroscopy*, 2021, **186**, 106307.

6 A. G. Seel, E. Zurek, A. J. Ramirez-Cuesta, K. R. Ryan, M. T. J. Lodge and P. P. Edwards, Low energy structural dynamics and constrained libration of $Li(NH_3)_4$, the lowest melting point metal, *Chem. Commun.*, 2014, **50**, 10778–10781.

7 F. Sacchetti, F. Demmel, E. Guarini and C. Petrillo, Complex dynamics in low electron density lithium ammonia solutions. Interacting modes revealed by comparing neutron and x-ray inelastic scattering, *Phys. Rev. Materials*, 2022, **6**, 115001.

8 W. J. Glover, R. E. Larsen and B. J. Schwartz, Simulating the Formation of Sodium:Electron Tight-Contact Pairs: Watching the Solvation of Atoms in Liquids One Molecule at a Time, *J. Phys. Chem. A*, 2011, **115**, 5887–5894.

9 W. J. Glover, R. E. Larsen and B. J. Schwartz, Nature of Sodium Atoms/(Na^+, e^-) Contact Pairs in Liquid Tetrahydrofuran, *J. Phys. Chem. B*, 2010, **114**, 11535–11543.

10 E. Zurek, X.-D. Wen and R. Hoffmann, (Barely) Solid $Li(NH_3)_4$: The Electronics of an Expanded Metal, *J. Am. Chem. Soc.*, 2011, **133**, 3535–3547.

11 V. V. Chaban and O. V. Prezhdo, Electron Solvation in Liquid Ammonia: Lithium, Sodium, Magnesium, and Calcium as Electron Sources, *J. Phys. Chem. B*, 2016, **120**, 2500–2506.

12 B. Baranyi and L. Turi, Excess electron solvation in ammonia clusters, *The Journal of Chemical Physics*, 2019, **151**, 204304.

13 I. R. Ariyarathna, F. Pawłowski, J. V. Ortiz and E. Miliordos, Aufbau Principle for Diffuse Electrons of Double-Shell Metal Ammonia Complexes: The Case of $M(NH_3)_4@12NH_3$, M = Li, Be^+, B^{2+}, *J. Phys. Chem. A*, 2020, **124**, 505–512.

14 I. R. Ariyarathna and E. Miliordos, Dative bonds versus electron solvation in tri-coordinated beryllium complexes: $Be(CX)_3$ [X = O, S, Se, Te, Po] and $Be(PH_3)_3$ versus $Be(NH_3)_3$, *Int J of Quantum Chemistry*, 2018, **118**, e25673.

15 I. R. Ariyarathna, S. N. Khan, F. Pawłowski, J. V. Ortiz and E. Miliordos, Aufbau Rules for Solvated Electron Precursors: $Be(NH_3)_4^{0,\pm}$ Complexes and Beyond, *J. Phys. Chem. Lett.*, 2018, **9**, 84–88.

16 I. R. Ariyarathna and E. Miliordos, Electronic and geometric structure analysis of neutral and anionic alkali metal complexes of the CX series (X = O, S, Se, Te, Po): The case of $M(CX)_{n=1-4}$ (M = Li, Na) and their dimers, *J Comput Chem*, 2019, **40**, 1344–1351.

17 I. R. Ariyarathna, N. M. S. Almeida and E. Miliordos, Stability and Electronic Features of Calcium Hexa-, Hepta-, and Octa-Coordinated Ammonia Complexes: A First-Principles Study, *J. Phys. Chem. A*, 2019, **123**, 6744–6750.

18 I. R. Ariyarathna and E. Miliordos, Superatomic nature of alkaline earth metal–water complexes: the cases of $Be(H_2O)0,+4$ and $Mg(H_2O)0,+6$, *Phys. Chem. Chem. Phys.*, 2019, **21**, 15861–15870.

19 Z. Jordan, S. N. Khan, B. A. Jackson and E. Miliordos, Can boron form coordination complexes with diffuse electrons? Evidence for linked solvated electron precursors, *Electron. Struct.*, 2022, **4**, 015001.

20 B. A. Jackson and E. Miliordos, The nature of supermolecular bonds: Investigating hydrocarbon linked beryllium solvated electron precursors, *The Journal of Chemical Physics*, 2022, **156**, 194302.

21 N. M. S. Almeida, F. Pawłowski, J. V. Ortiz and E. Miliordos, Transition-metal solvated-electron precursors: diffuse and 3d electrons in V(NH_3)0,±6, *Phys. Chem. Chem. Phys.*, 2019, **21**, 7090–7097.
22 N. M. S. Almeida and E. Miliordos, Electronic and structural features of octa-coordinated yttrium–ammonia complexes: the first neutral solvated electron precursor with eight ligands and three outer electrons, *Phys. Chem. Chem. Phys.*, 2019, **21**, 7098–7104.
23 S. N. Khan and E. Miliordos, Scandium in Neutral and Positively Charged Ammonia Complexes: Balancing between Sc^{2+} and Sc^{3+}, *J. Phys. Chem. A*, 2020, **124**, 4400–4412.
24 B. A. Jackson and E. Miliordos, Electronic and geometric structure of cationic and neutral chromium and molybdenum ammonia complexes, *The Journal of Chemical Physics*, 2021, **155**, 014303.
25 T. Furukawa, Y. Hirakawa, H. Kondo and T. Kanemura, Dissolution behavior of lithium compounds in ethanol, *Nuclear Materials and Energy*, 2016, **9**, 286–291.
26 N. Mozhzhukhina, M. P. Longinotti, H. R. Corti and E. J. Calvo, A conductivity study of preferential solvation of lithium ion in acetonitrile-dimethyl sulfoxide mixtures, *Electrochimica Acta*, 2015, **154**, 456–461.
27 K. Seng Tan, A. C. Grimsdale and R. Yazami, Synthesis and Characterization of Biphenyl-Based Lithium Solvated Electron Solutions, *J. Phys. Chem. B*, 2012, **116**, 9056–9060.
28 I. R. Ariyarathna and E. Miliordos, Geometric and electronic structure analysis of calcium water complexes with one and two solvation shells, *Phys. Chem. Chem. Phys.*, 2020, **22**, 22426–22435.
29 A. G. Seel, H. Swan, D. T. Bowron, J. C. Wasse, T. Weller, P. P. Edwards, C. A. Howard and N. T. Skipper, Electron Solvation and the Unique Liquid Structure of a Mixed-Amine Expanded Metal: The Saturated Li–NH_3–$MeNH_2$ System, *Angew Chem Int Ed*, 2017, **56**, 1561–1565.
30 H. Dong, Y. Feng and Y. Bu, Electron Presolvation in Tetrahydrofuran-Incorporated Supramolecular Sodium Entities, *J. Phys. Chem. A*, 2023, **127**, 1402–1412.
31 M. C. Cavanagh, R. E. Larsen and B. J. Schwartz, Watching Na Atoms Solvate into (Na^+, e^-) Contact Pairs: Untangling the Ultrafast Charge-Transfer-to-Solvent Dynamics of Na^- in Tetrahydrofuran (THF), *J. Phys. Chem. A*, 2007, **111**, 5144–5157.
32 I. R. Ariyarathna, F. Pawłowski, J. V. Ortiz and E. Miliordos, Molecules mimicking atoms: monomers and dimers of alkali metal solvated electron precursors, *Phys. Chem. Chem. Phys.*, 2018, **20**, 24186–24191.
33 V. W. Day, Md. A. Hossain, S. O. Kang, D. Powell, G. Lushington and K. Bowman-James, Encircled Proton, *J. Am. Chem. Soc.*, 2007, **129**, 8692–8693.
34 O. Klein, F. Aguilar-Parrilla, J. M. Lopez, N. Jagerovic, J. Elguero and H.-H. Limbach, Dynamic NMR Study of the Mechanisms of Double, Triple, and Quadruple Proton and Deuteron Transfer in Cyclic Hydrogen Bonded Solids of Pyrazole Derivatives, *J. Am. Chem. Soc.*, 2004, **126**, 11718–11732.
35 A. D. McElroy, J. Kleinberg and A. W. Davidson, Metallic Aluminum in Solution in Liquid Ammonia, *J. Am. Chem. Soc.*, 1950, **72**, 5178–5180.
36 J. L. Dye, The alkali metals: 200 years of surprises, *Phil. Trans. R. Soc. A.*, 2015, **373**, 20140174.
37 M. J. Frisch et al., *Gaussian-09 Revision D.01*, 2013.
38 M. J. Frisch et al., *Gaussian-16 Revision C.01*, 2019.
39 A. D. Becke, Density-functional thermochemistry. III. The role of exact exchange, *The Journal of Chemical Physics*, 1993, **98**, 5648–5652.
40 C. Lee, W. Yang and R. G. Parr, Development of the Colle-Salvetti correlation-energy formula into a functional of the electron density, *Phys. Rev. B*, 1988, **37**, 785–789.
41 S. H. Vosko, L. Wilk and M. Nusair, Accurate spin-dependent electron liquid correlation energies for local spin density calculations: a critical analysis, *Can. J. Phys.*, 1980, **58**, 1200–1211.
42 P. J. Stephens, F. J. Devlin, C. F. Chabalowski and M. J. Frisch, Ab Initio Calculation of Vibrational Absorption and Circular Dichroism Spectra Using Density Functional Force Fields, *J. Phys. Chem.*, 1994, **98**, 11623–11627.

43 T. Yanai, D. P. Tew and N. C. Handy, A new hybrid exchange–correlation functional using the Coulomb-attenuating method (CAM-B3LYP), *Chemical Physics Letters*, 2004, **393**, 51–57.
44 S. Grimme, S. Ehrlich and L. Goerigk, Effect of the damping function in dispersion corrected density functional theory, *Journal of Computational Chemistry*, 2011, **32**, 1456–1465.
45 A. D. McLean and G. S. Chandler, Contracted Gaussian basis sets for molecular calculations. I. Second row atoms, *Z* =11–18, *The Journal of Chemical Physics*, 1980, **72**, 5639–5648.
46 R. Krishnan, J. S. Binkley, R. Seeger and J. A. Pople, Self-consistent molecular orbital methods. XX. A basis set for correlated wave functions, *The Journal of Chemical Physics*, 1980, **72**, 650–654.
47 B. G. Janesko, G. Scalmani and M. J. Frisch, How far do electrons delocalize?, *The Journal of Chemical Physics*, 2014, **141**, 144104.
48 B. G. Janesko, G. Scalmani and M. J. Frisch, Quantifying solvated electrons' delocalization, *Phys. Chem. Chem. Phys.*, 2015, **17**, 18305–18317.
49 B. G. Janesko, Topological analysis of the electron delocalization range, *J. Comput. Chem.*, 2016, **37**, 1993–2005.
50 B. Silvi and A. Savin, Classification of chemical bonds based on topological analysis of electron localization functions, *Nature*, 1994, **371**, 683–686.
51 S. Noury, X. Krokidis, F. Fuster and B. Silvi, Computational tools for the electron localization function topological analysis, *Computers & Chemistry*, 1999, **23**, 597–604.
52 T. Lu and F. Chen, Multiwfn: A multifunctional wavefunction analyzer, *J Comput Chem*, 2012, **33**, 580–592.
53 J. A. Howard, H. A. Joly, P. P. Edwards, R. J. Singer and D. E. Logan, Electron paramagnetic resonance study of the reaction of ground-state aluminum atoms with ammonia in a rotating cryostat, *J. Am. Chem. Soc.*, 1992, **114**, 474–477.
54 B. Gaertner and H.-J. Himmel, Structure and Bonding in the Aluminum Radical Species Al·NH_3, $HAlNH_2$, $HAlNH_2 \cdot NH_3$, and $Al(NH_2)_2$ Studied by Means of Matrix IR Spectroscopy and Quantum Chemical Calculations, *Inorg. Chem.*, 2002, **41**, 2496–2504.
55 T. Di Palma, A. Latini, M. Satta, M. Varvesi and A. Giardini, Pulsed laser reactive ablation of Al in an ammonia atmosphere: photoionization thresholds and structures of Al–NH3 clusters, *Chemical Physics Letters*, 1998, **284**, 184–190.
56 E. R. Johnson, A. Otero-de-la-Roza and S. G. Dale, Extreme density-driven delocalization error for a model solvated-electron system, *The Journal of Chemical Physics*, 2013, **139**, 184116.
57 Q.-W. Song, R. Ma, P. Liu, K. Zhang and L.-N. He, Recent progress in CO_2 conversion into organic chemicals by molecular catalysis, *Green Chem.*, 2023, **25**, 6538–6560.
58 R. J. Detz, C. J. Ferchaud, A. J. Kalkman, J. Kemper, C. Sánchez-Martínez, M. Saric and M. V. Shinde, Electrochemical CO_2 conversion technologies: state-of-the-art and future perspectives, *Sustainable Energy Fuels*, 2023, **7**, 5445–5472.
59 B. A. Jackson, S. G. Dale, M. Camarasa-Gómez and E. Miliordos, Introducing Novel Materials with Diffuse Electrons for Applications in Redox Catalysis and Quantum Computing via Theoretical Calculations, *J. Phys. Chem. C*, 2023, **127**, 9295–9308.
60 H. Huang, L. Xue and Y. Bu, Multifunctional Roles of Clathrate Hydrate Nanoreactors for CO_2 Reduction, *Chemistry A European J*, 2023, **29**, e202302253.
61 Y. Meng, H. Huang, Y. Zhang, Y. Cao, H. Lu and X. Li, Recent advances in the theoretical studies on the electrocatalytic CO2 reduction based on single and double atoms, *Front. Chem.*, 2023, **11**, 1172146.
62 N. Davison, J. A. Quirk, F. Tuna, D. Collison, C. L. McMullin, H. Michaels, G. H. Morritt, P. G. Waddell, J. A. Gould, M. Freitag, J. A. Dawson and E. Lu, A room-temperature-stable electride and its reactivity: Reductive benzene/pyridine couplings and solvent-free Birch reductions, *Chem*, 2023, **9**, 576–591.